Methods 98 (2016) 134–142

Contents lists available at ScienceDirect

Methods

journal homepage: www.elsevier.com/locate/ymeth

Single molecule approaches for quantifying transcription and degradation rates in intact mammalian tissues

Keren Bahar Halpern, Shalev Itzkovitz *

Department of Molecular Cell Biology, Weizmann Institute of Science, Rehovot, Israel

ARTICLE INFO

Article history:
Received 6 September 2015
Received in revised form 15 November 2015
Accepted 19 November 2015
Available online 29 November 2015

Keywords:
Single molecule
Systems biology
Transcription

ABSTRACT

A key challenge in mammalian biology is to understand how rates of transcription and mRNA degradation jointly shape cellular gene expression. Powerful techniques have been developed for measuring these rates either genome-wide or at the single-molecule level, however these techniques are not applicable to assessment of cells within their native tissue microenvironment. Here we describe a technique based on single molecule Fluorescence *in-situ* Hybridization (smFISH) to measure transcription and degradation rates in intact mammalian tissues. The technique is based on dual-color libraries targeting the introns and exons of the genes of interest, enabling visualization and quantification of both nascent and mature mRNA. We present a software, TransQuant, that facilitates quantifying these rates from smFISH images. Our approach enables assessment of both transcription and degradation rates of any gene of interest while controlling for the inherent heterogeneity of intact tissues.

1. Introduction to the technique

The levels of cellular mRNA are governed by two highly controlled processes – transcription and mRNA degradation. The balance between these processes dictates not only the steady state transcript levels but also the gene's response time [1,54,63,64,79] and susceptibility to noise [3,57]. Measurements of degradation rates of endogenous mRNAs have been performed in a number of ways, including usage of transcriptional inhibitors such as actinomycin D, which interferes with transcription by intercalating into DNA [44,54], and 5,6-dichloro-1β-1-ribofuranosylbenzimidazole (DRB), which interacts directly with the RNA polymerase II transcription apparatus [12,21]. Genome-wide measurements of gene expression at sequential time points following such transcription inhibition enable inference of mRNA lifetimes. A limitation of this methodology is that transcription inhibition often introduces significant changes to cell physiology, e.g. to the transcription of components of RNA degradation machinery [6,26,61]. As a result, mRNA lifetimes obtained in such experiments may not necessarily reflect the true stability of the mRNAs.

Other techniques to estimate rates of transcription and degradation rely on combined measurements of both newly transcribed RNA molecules and total RNA. These include techniques that capture the RNA bound to actively transcribing Pol2, such as Nascent-seq [35,45,60], NET-seq [15,43,50] and GRO-seq [16]. A complementary approach to estimate these rates on a genome-wide basis is metabolic labeling of RNA with 4-thiouridine (4sU) or 5′-bromo-uridine (BrU), modified uridines that enable specific pull-down of recently transcribed RNA from the overall RNA population, with minimal interference to normal cell growth [30,54,55]. These powerful techniques provide a genome-wide view of transcription and degradation; however, they work on bulk measurements, thus providing an average picture of these rates and potentially missing the variability between sub-populations. Accounting for such variability is important when samples are heterogeneous [27,32]. In such cases techniques that enable single-cell measurements are required.

A complementary set of strategies to infer transcription and degradation rates that focus on single cells apply imaging techniques to follow individual RNA molecules inside living cells. The MS2–GFP technique [7,10,24,53] uses a modified RNA that contains multiple tandem sequences recognized by the MS2 bacteriophage coat protein. A simultaneously expressed MS2–GFP fusion protein localizes on the tandem repeats yielding a bright fluorescent spot, which can be followed in time within the cells. Another method that allows imaging of individual mRNA is by hybridization of molecular beacons (MBs) to multiple tandem repeats engineered into the desired mRNA [11,48,75,76]. Molecular beacons are hairpin shaped molecules with an internally quenched fluorophore, the fluorescence of which is restored when they bind to a target nucleic acid sequence. Although these techniques offer

* Corresponding author.
E-mail address: shalev.itzkovitz@weizmann.ac.il (S. Itzkovitz).

http://dx.doi.org/10.1016/j.ymeth.2015.11.015
1046-2023/

unprecedented spatial and temporal resolution they require manipulations such as transfection of constructs that incorporate the modified RNA (MS2–GFP) or microinjection of the fluorescent probes into the cells, thus applicable only to living cultured cells.

Extracting the rates of transcription and degradation of cells that reside within their natural tissue microenvironment is an outstanding challenge. This is particularly important in heterogeneous tissues, which invariably contain different cell types and diverse sub-populations. Tissues are often polarized by morphogens or blood flow and thus the location of cells within a tissue is a key determinant of their gene expression states [27]. Accounting for this spatial variability requires techniques for quantitative single-cell analysis without dissociating the tissue. The single molecule Fluorescence *in-situ* Hybridization (smFISH) technique facilitates visualization of mRNA molecules in fixed cells or tissues [19,34,39,40,42,51,57,58,71,78]. This technique relies on the specific hybridization of libraries of short DNA sequences that are complementary to a specific target RNA sequence that are all coupled to the same fluorophore. Binding of multiple probes to the same transcript yields a bright dot, indicative of a single mRNA transcript. This method has been used in bacteria [42,65,66], yeast [42,71,80], mammalian cells [34,57] and recently even in intact tissues [3,28,29,39,78]. Here we describe a modification of this technique [3] that enables not only measurements of the amount of mRNA per cell but also quantification of the rates of transcription and mRNA degradation at the single-molecule, single-cell level in intact tissues. We provide a simple software, TransQuant, that implements our method for estimating these rates from smFISH microscopy images.

2. Theory and rational

The dynamics of mRNA production can be modeled as a first-order process [1]:

$$dX/dt = \beta - \delta X \tag{1}$$

where β is the cellular transcription rate, in units of mRNA/h, δ is the rate of mRNA degradation (1/h) and X the number of cytoplasmic mRNA molecules. Under steady state conditions, defined as conditions where β and δ have been constant for enough time so that temporal changes in X are negligible, the average number of mRNA per cell can be found by setting Eq. (1) to 0 ($dX/dt = 0$):

$$X_{st} = \beta/\delta \tag{2}$$

Eq. (2) indicates that a given level of cellular mRNA can be achieved by either high rates of both transcription and degradation or low rates of both transcription and degradation. Using Eq. (2) we can infer mRNA degradation rates δ from combined measurements of β and X_{st}:

$$\delta = \beta/X_{st} \tag{3}$$

The number of mRNA per cell in steady state, X_{st}, can be obtained using smFISH by identifying individual mRNA dots in 3D images and assigning them to cells. Obtaining the transcription rate, β, requires identification of the transcription sites (TS), and quantification of the average number of Pol2 molecules actively transcribing (termed 'polymerase occupancy', M). Assuming that Pol2 elongates at a constant rate v and immediately releases the nascent transcript at the 3′ end of the gene, the rate of mRNA production from a TS, denoted by μ, is:

$$\mu = M \cdot v/L \tag{4}$$

where L is the length of the gene and M is the average number of Pol2 molecules on a typical locus (Fig. 1A). Transcription is generally a bursty process [3,4,8,9,13,17,20,24,33,49,52,56,69], and promoters are thought to stochastically switch between non-active and active transcriptional states, so in general only a fraction f of the chromosomal copies in the cell will be active. As a result, the average transcription rate per cell that contains n chromosomal copies, β, is:

$$\beta = n \cdot f \cdot \mu = n \cdot f \cdot M \cdot v/L \tag{5}$$

where we have used Eq. (4) for μ. Eq. (5) assumes that the velocity of Pol2 is known (this will be discussed in the computational methods section) and that all nascent mRNA end up in the cytoplasm, neglecting nuclear degradation of improperly spliced mRNA [22].

Eq. (5) indicates that measurements of the cellular ploidy (n), the fraction of chromosomal copies that are transcriptionally active (f), and the average number of Pol2 molecules on a given TS (M) can be used to infer cellular transcription rate (β). Additionally measuring the average number of mRNA per cell at steady state (X_{st}) will facilitate inferring degradation rates using Eq. (3) (Fig. 1B). We will next describe our smFISH approach for imaging individual mature and nascent mRNA in intact mouse tissue sections and for inferring the rates of transcription and mRNA degradation.

3. Establishing image based analysis of transcription and degradation rates in intact mammalian tissues

The detailed protocol of single molecule mRNA detection and counting in mammalian tissues was previously published [41]; here we describe how to modify the smFISH technique in order to quantify the active sites of transcription and to extract dynamic gene expression properties in intact mammalian tissues (Fig. 1C). In order to visualize nascent mRNA, one must locate and quantify TS. A common approach for identifying active transcription sites using smFISH is to seek bright dots that reside in the nucleus [39,80]. Since several Pol2 molecules may be actively engaged in transcription of the target gene of interest, and since each Pol2 will carry a tail of partially transcribed mRNA (Fig. 1A), the local concentration of smFISH fluorescent probes will be higher in a TS compared to a single cytoplasmic mRNA, thus yielding a brighter dot. While this strategy seems to work well for organisms such as yeast and drosophila, the abundance of nuclear mRNA molecules and the low Pol2 occupancy in many of the endogenous genes prohibit unambiguous identification of TS in mammalian cells using this approach (Fig. 1D).

Identifying TS can be achieved by labeling not only the exons of the transcripts of interests but also the introns [38]. Introns are generally spliced and degraded co-transcriptionally [2,23,36,46,72], therefore intact stretches of introns only reside at the active sites of transcription. To utilize this fundamental property of mammalian transcription we use two smFISH probe libraries coupled to spectrally resolvable fluorophores; one that targets the exons of the gene of interest and a second library that targets the introns. The intronic dot facilitates unambiguous identification of the TS, whereas the exonic dot enables quantification of the average Pol2 occupancies (Fig. 1C and D). In the following sections we describe in details our protocol steps, summarized in Fig. 2.

4. Tissue processing

To obtain precise measurements of the gene expression parameters, RNA integrity must be preserved during the tissue handling. To this end, we excise the tissue immediately after sacrification of the animal and place it in 4% PFA for fixation (as described in [41]). After cryopreservation, tissues are placed in OCT molds and stored frozen at −80 °C. For visualization of full nuclei, thick tissue sections (25 μM) are mounted on poly-L lysine coated #1 coverslips. The

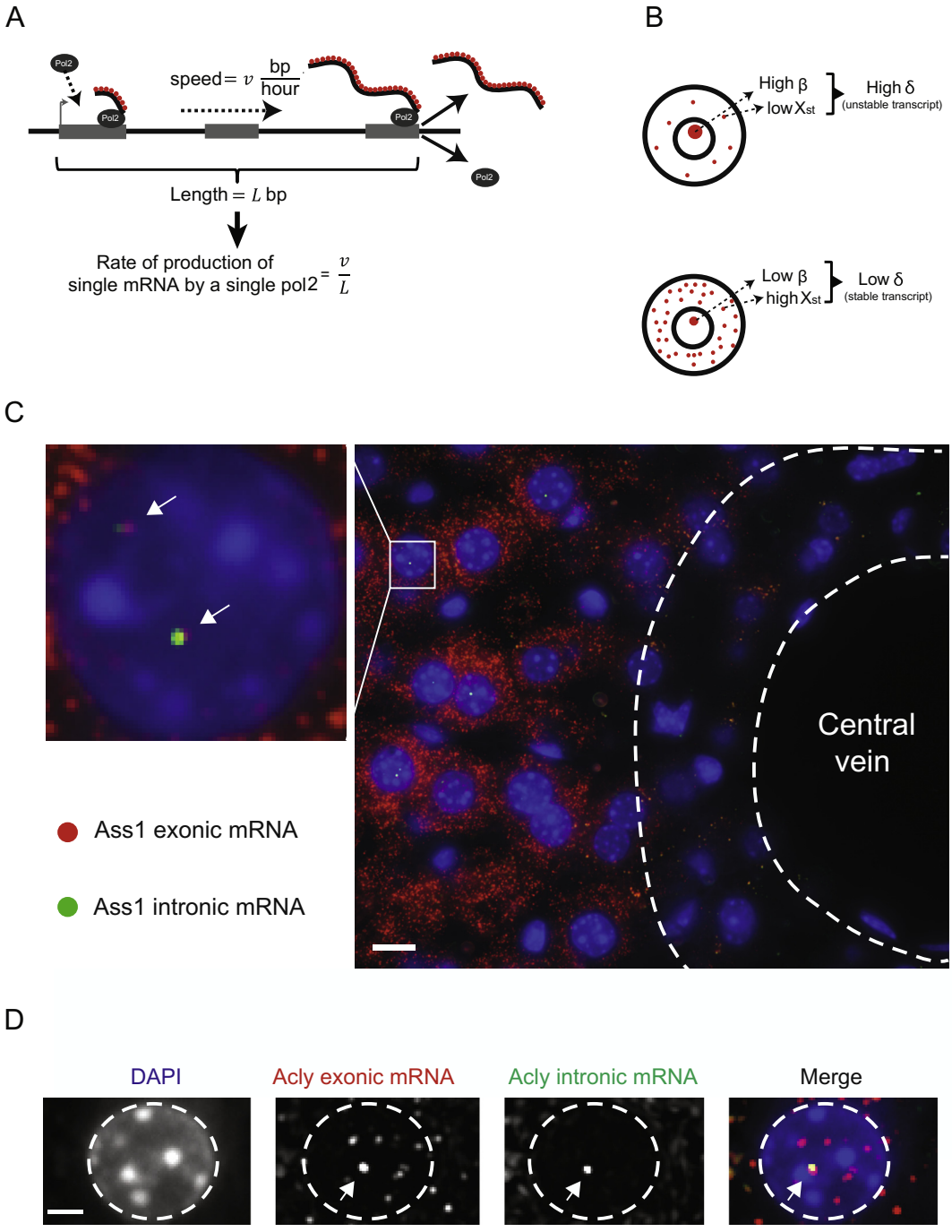

Fig. 1. Single molecule approach for measuring gene expression parameters. (A) Calculation of transcription rate from a single RNA polymerase. v is the speed of RNA polymerase; L is the length of the full gene. Red circles represent single probes attached to the newly synthetized RNA molecule (black curve). The rate of production of a single RNA molecule equals the ratio between RNA polymerase speed and the length of the gene. (B) Diagram of two cells with different expression parameters. Each red dot represents a single RNA molecule in the cytoplasm. A larger red dot represents an active transcription site in the nucleus. The top cell has low levels of mRNA (X_{st}). The bright nuclear dot represents an active transcription site with high transcription rate (β). Combination of these two parameters indicates that the mRNA is unstable with a high degradation rate (δ). The bottom cell has high levels of mRNA (X_{st}) and a nuclear active transcription site with low transcription rate (β). Combination of these two parameters indicates that the mRNA is stable and has a low degradation rate (δ). (C) Example of the smFISH approach for estimating transcription and degradation rates in the intact liver. Red dots are single mRNA molecules of Argininosuccinate synthase 1 (Ass1) green dots are intronic library marking active TS. Blue – DAPI-stained nuclei. Arrows mark two transcription sites. Inner dashed curve delineates the central vein, outer dashed curve delineates the pericentral zone, where Ass1 expression is strongly repressed. By excluding this region from the analysis, the *in-situ* approach enables analysis of a tissue region where expression can be considered homogenous. Scale bar: 10 μm. (D) Hybridization with both intronic and exonic libraries is necessary to unambiguously identify TS in mammalian cells. Red channel is exonic probe library of ATP citrate lyase (Acly), green channel is the intronic probe library, DAPI-stained nucleus is in blue. Arrow points at a TS, dashed circles mark the nucleus. Note that the nucleus has several spliced mRNA and only a single TS identified by the intronic library. Scale bar: 2 μm.

sections are left to air-dry for around 10 min and placed on dry ice until fixation. After sectioning, the tissues are post-fixed with 4% PFA, then washed once with cold PBS and incubated in 70% at 4 °C for at least 2 h before proceeding to hybridization. Importantly, thinner sections (e.g. 6 μM) can also be used, with a modified computational algorithm described below (termed the 'pooled method'). Thick sections should be handled with care during the washing steps as they have a higher tendency to detach from the cover slips.

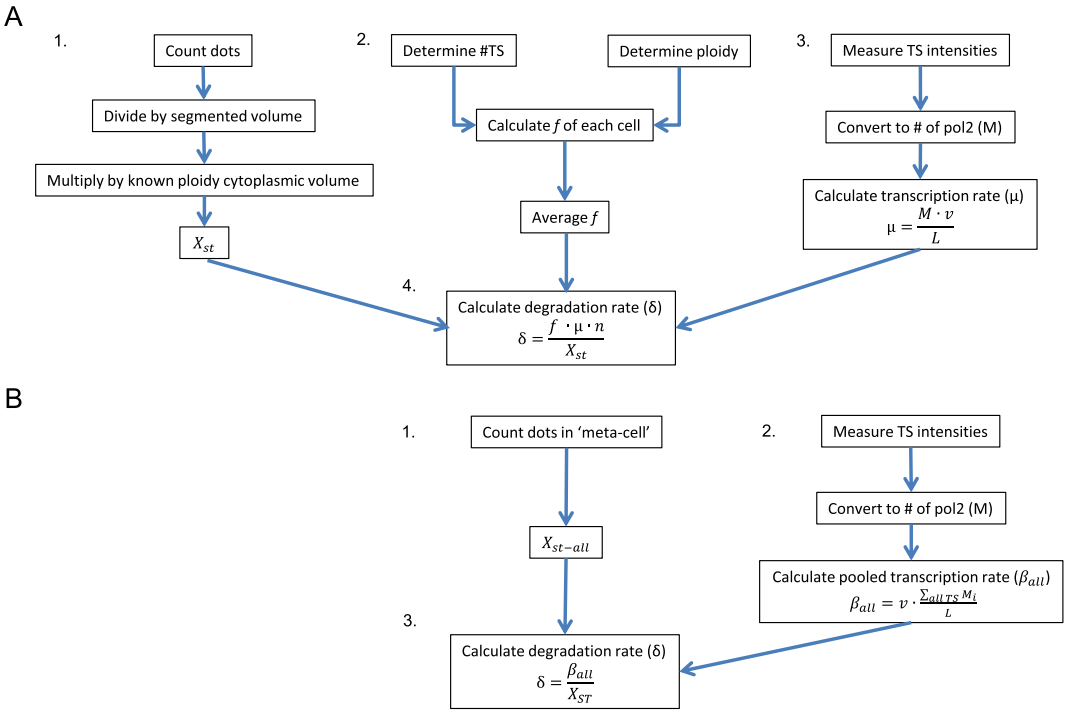

Fig. 2. Common steps in image based analysis of transcription and degradation rates. (A) Flow chart of the steps in the 'single-cell method' for calculation of gene expression parameters. f is the average fraction of active transcription sites, M is the average Pol2 occupancy on single active TS, v is the speed of Pol2, μ is the calculated transcription rate, X_{st} is the average number of mRNA molecules in each cell, δ is the inferred degradation rate. (B) Flow chart of the steps in the 'pooled method' for calculating gene expression parameters. β_{all} is the pooled transcription rate from all active TS in an imaged field, $X_{st\text{-}all}$ is the number of all mRNA molecules in an imaged field.

5. Probe design and imaging

5.1. Probe library design and considerations

Probe libraries are designed using Stellaris® Probe Designer Access (Biosearch technologies). The designer finds a library of probes that are complementary to sequential parts of the gene of interest, have uniform GC content and at least 2 nucleotide spacing between sequential probes. It is recommended to use the organism-specific masking option to avoid non-specific off-target binding of the probes. Each library is comprised of 48–96 probes which are designed to be complementary to the exons or the introns of the gene of interest. Ideally, the intron probe library should contain probes that are complementary to as many introns of the gene of interest as possible, to ensure detection of all active TS. To understand this effect, consider a long gene that includes an intron at the 5′ region of the gene as well as other introns more downstream along the gene. If probes are designed exclusively for the 5′ intron there could be situations where a single Pol2 molecule has advanced well into the gene and splicing and consequent degradation of the intron has already occurred. In these cases we will not observe the intronic dot and miss some TS, leading to underestimation of the transcription rate (Fig. 3A).

Probe libraries are either ordered coupled and purified from Biosearch, or alternatively ordered in a plate format with a 3′ amide modification and pooled and coupled in-house [65]. Since transcription sites are expected to appear in both the intron and exon channel one must avoid bleed-through from one channel to another, otherwise non-TS nuclear mRNA might be mistaken for true TS. We therefore use two fluorophores that are spectrally separated from each other. We recommend 6-carboxytetramethylrhodamine succinimidyl ester (TAMRA – emission 580 nm) for the intron library and Cy5 (emission 670 nm) for the exon library. In the third fluorescent channel, normally Alexa594, one can use smFISH probes for an additional gene; however it is important that this gene will not have bright transcription sites as the Alexa594 signal could potentially bleed through to both the cy5 and TMR channels. In liver tissue we use ActB probe library coupled to Alexa594 fluorophore as a positive control, since this gene is ubiquitously expressed but has rare, relatively non-intense transcription sites [3].

5.2. Imaging setup

All Images are taken with a Nikon Ti-E inverted fluorescence microscope equipped with a ×100 oil-immersion objective and a Photometrics Pixis 1024 CCD camera using MetaMorph software (Molecular Devices, Downington, PA). We use a wide-spectrum light source (either Prior Lumen 220Pro or Nikon Intensilight). In liver tissue sections quantification of transcription sites and nuclear volume are performed on stacks of 45 optical sections spaced 0.3 μm apart. It is important to image and analyze regions of the tissue that could be assumed to be uniform in the measured parameters. For example the liver is composed of repeating anatomical units termed lobules that are polarized by blood flowing from portal nodes to central veins. In this tissue uniform regions could be the hepatocytes that surround the portal nodes, where the microenvironment is distinctly different from that at the central vein region (Fig. 1C).

A potential problem that arises when imaging thick tissue sections is the fading of the fluorescence signal as one moves the focal plane into the depth of the tissue and farther from the coverslip. This decrease in fluorescent signal, due to scattering from the tissue, can lead to a decline in the number of detectable dots along the Z-direction. Therefore, although the entire section is imaged, we recommend quantifying the mRNA concentrations based only on the first 10 optical sections (3 μm), where such scattering effects are negligible.

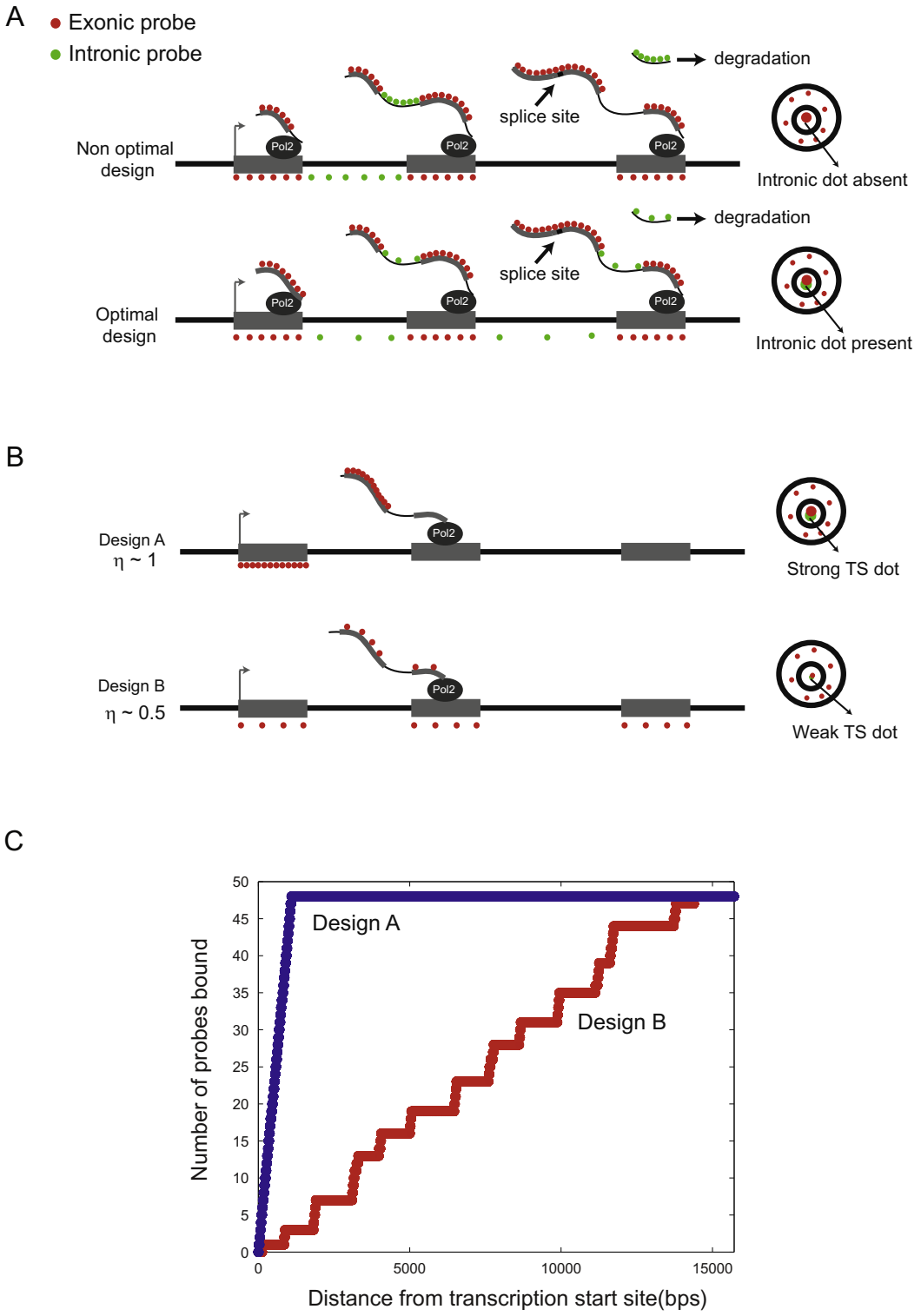

Fig. 3. Considerations in probe library design. (A) Designing an intronic probe library that spans all of the introns minimizes the chance to miss TS. Red circle represents a single exonic probe; green circle is a single intronic probe. Top illustration shows the less optimal design of the intron library in which all probes are designed to be complementary to the first intron. The first intron may be spliced out early, and thus the TS will only exhibit an exonic dot (cell illustration on the right). In such case the TS will be missed leading to underestimation of transcription rate. The second design is preferable since the intronic probe library is designed to target introns throughout the length of the gene. (B) The conversion factor η is based on the spread of the exonic probe library along the gene. Design A will lead to $\eta \sim 1$ indicating that an average Pol2 molecule will yield dot intensity that is equivalent to a cytoplasmic dot having the full set of 48 probes bound. Design B will lead to $\eta \sim 0.5$ indicating that an average Pol2 molecule will yield a dot that is approximately half the intensity of a cytoplasmic dot having only half of the 48 probes bound. (C) Plot illustrates the number of exonic probes bound on a nascent mRNA attached to Pol2 molecules at different locations along the gene. Blue curve illustrates a library such as design A, red curve illustrates a library such as design B.

We recommend acquiring Z-stacks in 5 different channels, three smFISH channels, DAPI channel for nuclear detection and GFP channel for imaging phalloidin-FITC membrane stains to reveal cellular boundaries. When imaging three smFISH channels the filter cubes must be chosen carefully to minimize bleed through between the different channels. Table 1 lists the filter cubes of choice. Note that we image the cy5 channel with a cy5.5 filter cube. Although this filter cube is sub-optimal for detection of cy5 emission since it is shifted farther to the red compared to the cy5 emission peak it minimizes bleed-through from the A594 channel and still provides cy5 dot-detection that is not inferior to the cy5 filter cube. Typical exposure times in our optical setup are around 1–3 s for the smFISH channels. Our mounting medium includes scavengers of Reactive Oxygen Species (ROS) [41], which are critical to avoid bleaching of the cy5 fluorophores during the relatively long exposure times applied.

Since we are detecting diffraction-limited dots it is important to image with a spatial resolution that exceeds the diffraction limit [27]. Using a 100X objective and a CCD of 1024 * 1024 pixels with a physical size of 13 mm we obtain a pixel size of 0.13 μm which maintains this condition.

6. Computational methods

We describe two methods for extracting transcription and degradation rates using smFISH. In the first (termed 'single-cell method') we quantify the average amount of mRNA per cell as well as the average transcription rate per cell by imaging thick tissue sections, facilitating detection of the entire nuclear volume. In the second method (termed 'pooled method') we quantify the ratio between overall transcription rate and mRNA levels by imaging thin sections and pooling all cells in an imaging field. The first approach is ideal when single cells can be clearly segmented, e.g. in tissues such as the liver, whereas the second approach is more suitable for tissues such as the intestinal epithelium where cells are often overlapping and cannot be easily segmented. We provide a software, TransQuant (Supplementary material), that implements dot counting, as well as rates estimation by the pooled method.

6.1. Single cell method

Fig. 2A presents a flowchart of the computational pipeline for the single-cell method. This method entails quantification of the fraction of chromosomal copies that are actively transcribing (f, (Fig. 2A2)), the average rate of mRNA production from each active TS (Fig. 2A3) and the average numbers of cytoplasmic mRNA molecules per cell (X_{st}, (Fig. 2A1)).

The output of the imaging session is a set of three dimensional image stacks. The first computational step is to use image processing to count the number of dots in these three-dimensional stacks. We perform dot counting and cell segmentation using the Matlab based GUI TransQuant (Supplementary material). Cell segmentation is based on FITC-phalloidin membrane staining and DAPI nuclear staining.

Table 1
Filter cubes used for the three fluorescent smFISH channels.

Fluorophore	Company	Filter cube
Cy5	Chroma	49022-ET Cy5.5 filter cube
Alexa594	Omega optical	Custom cube consisting of 590DF10 excitation filter, 610DRLP dichroic filter and 630DF30 emission filter
TMR	Omega optical	XF204 filter cube

Eq. (3) requires measurements of the average number of mRNA molecules per cell at steady state (X_{st}). While directly counting all mRNA molecules in a cell is feasible when cells are spread out on a coverslip and are thus completely included in a few Z-stacks, large cells in intact tissues such as liver may require imaging to a depth of 10 μm or more. The optical aberrations in the tissue render it impossible to accurately count dots at a depth of more than 3–4 μm from the coverslip. To alleviate this problem we first compute the cytoplasmic mRNA concentration based on the Z-stacks for which reliable dots can be detected, and then multiply this concentration by the cellular volume, taken from literature.

Detection of active TS (Fig. 2A2) can in principle be performed fully automatically by computationally detecting exonic and intronic dots that are nuclear and physically closer than some critical threshold [3]. This approach, however, has some caveats. There are situations in which the transcribed gene is long and rather than observing diffraction-limited dots, we observe fluorescence over several image voxels. In addition, when transcription rate is extremely low, dots may be barely detected automatically. This could happen in cases where a single Pol2 is actively transcribing but is situated at the beginning of the gene, and thus has a short mRNA tail where only few probes can bind. In such cases, dots will be much dimmer than the mature mRNA dots in which all the designed probes can bind.

Due to these and other factors we recommend manually identifying the double-labeled nuclear TS dots, using software such as FIJI [62] (see TransQuant, Supplementary materials). Once TS have been identified the fraction of active TS per cell is the ratio between the number of TS per cell and the expected number of chromosomal copies. These would in general be two for diploid cells but potentially higher, e.g. in a polyploid tissue such as the mammalian liver or in rapidly cycling cells where some cells are in G2. When computing f, it is important to use only the nuclei for which the entire 3D volume is included in the image stacks. We validate this by reconstructing the nuclear area profile based on the DAPI images and removing nuclei that exhibit a maximum of the cross-section profile that is too close to the stack edges [3].

The last parameter to be measured is the average transcription rate from active TS, μ (Fig. 2A3). To estimate this rate we must first determine the average polymerase occupancy of a TS, the number of Pol2 molecules situated on the chromosomal locus that is actively involved in transcription (M, Eq. (5)). The higher M the brighter would be the TS dot. To estimate M we quantify the intensity of both the cytoplasmic exonic dots ($I_{E\text{-}nonTS}$) as well as the intensity of the TS exonic dots ($I_{E\text{-}TS}$). To this end, we integrate the background-subtracted values of all dot pixels in the optical Z-section where the dot is brightest [3]. We next use the following formula to obtain M:

$$M = I_{E\text{-}TS}/(\eta \cdot \kappa \cdot median(I_{E\text{-}nonTS})) \quad (6)$$

where $\lceil x \rceil$ is the ceiling operator, the lowest integer number larger than x, $I_{E\text{-}TS}$ is the intensity of the TS dot appearing in the exonic channel and the median is taken over non-TS that are in the same optical section as the maximal-intensity section of the TS. Eq. (6) has two important conversion factors, one for the spread of the exonic probes along the gene of interest (η) and another for the inferred occupancies (κ).

The first conversion factor, η, incorporates the physical location of each probe in the smFISH library along the gene of interest. To understand the importance of this conversion, consider the difference between a library design in which all 48 exonic probes bind the first 10% length of the gene and another design in which the 48 probes are evenly spread along the gene. If the average Pol2 molecule is situated in the middle of the gene the first design will yield a dot intensity that is almost equivalent to a cytoplasmic dot having the full set of 48 probes bound, whereas the second design

will yield a dot that is approximately half the intensity (Fig. 3B and C). The equation describing the correction factor is:

$$\eta = \left(\frac{1}{L}\right)\sum_{i=1}^{L}\frac{N(i)}{N(L)} \tag{7}$$

where L is the length of the gene and $N(i)$ is the number of probes bound to a nascent mRNA attached to a Pol2 molecule that has reached position i on the gene. $N(L)$ is the full complement of 48 library probes, representing the intensity of a cytoplasmic dot. η is close to 1 when probes are designed to target the first part of the gene, approximately 0.5 when probes are uniformly spread along the target gene and close to 0 if probes mainly target the last part of the gene (Fig. 3B). η can be calculated using the TransQuant software (Supplementary materials).

The second conversion factor, κ, is obtained by using Eq. (6) on a fully mature cytoplasmic mRNA dot (for which we use $\eta = 1$). Although the 'occupancy' of such a dot should be 1 the inferred occupancy is in fact higher because of the ceiling operator in Eq. (6). Thus the equation for this correction factor is:

$$\kappa = I_{E\text{-}nonTS}/(median(I_{E\text{-}nonTS})) \tag{8}$$

Once the average occupancy of a TS has been determined using Eqs. (6)–(8) we convert this to transcription rate using Eq. (4). The average speed of Pol2 can be taken from literature [21,31] or calibrated in-house [3]. Importantly, our estimates assume that all nascent mRNA that are localized on the TS are attached to Pol2 molecules that are actively proceeding at a constant rate and that the fully transcribed mRNA is immediately released when the Pol2 reaches the 3′ end of the gene. When this is not the case our analysis may lead to over-estimation of the transcription rates. These assumptions can be validated by comparing dot intensities of dual color libraries that target the first and last exonic parts of the gene of interest [3].

Once the average number of cytoplasmic mRNA dots per cell (X_{st}), the average probability of a chromosomal locus to be transcriptionally active (f) and the average transcription rate from such active TS (μ) have been estimated we use Eq. (5) to extract β, the average cellular transcription rate. We also use Eq. (3) to obtain the degradation rate, the ratio between transcription rate and average cytoplasmic mRNA.

6.2. Pooled method

An alternative to the single-cell method that is more applicable to thin sections and to conditions where individual nuclei and cells cannot be easily segmented is to treat the entire imaging field as a 'meta-cell', thus computationally pooling all transcription sites and mRNA dots. In this method we first count all mRNA molecules in the first 10–15 stacks of the imaging field, $X_{st\text{-}all}$ (Fig. 2B1). Next, we manually mark all active TS in the quantified stacks of this imaging field using FIJI, by identifying the nuclear double-labeled dots. We then use Eq. (5) to obtain the Pol2 occupancy of each TS dot, M_i, and compute the pooled transcription rate (Fig. 2B2) as:

$$\beta_{all} = v \cdot \frac{\sum_{allTS} M_i}{L} \tag{9}$$

Finally we compute the degradation rate as:

$$\delta = \frac{\beta_{all}}{X_{st\text{-}all}} \tag{10}$$

As in the single-cell method, the pooled method also enables differentiating between low transcription rates of many active TS (high f, low μ) and high transcription rates of a few "bursting" active TS (low f, high μ), however with lower accuracy. Unlike the single-cell method for which f is directly computed, in the pooled method one can manually count the number of cells in the imaging field and divide the total number of active TS by the expected number. While this provides a reasonable estimate of f in uniform tissues, this approach may be error-prone when there is high single-cell variability in the ploidy levels of cells, e.g. in a polyploid tissue such as the liver.

The pooled method enables inference of the key parameters without the need to segment cells, a process that involves manual labor. In addition, it requires only thin sections, which are easier to cryo-section and require less delicate handling during the protocol washing steps. However, unlike the single-cell method it provides only coarse information about the heterogeneity of the tissue, mainly controlling for the broad location of the cells within the tissue. To avoid mixing cells of different types one can manually segment 'excluded regions' in the image where dots are not counted, e.g. non-paranchymal cells in the liver or non-epithelial cells in the intestine. The pooled method is implemented in TransQuant (Supplementary materials).

7. Limitations and outlook

Finally, we note some assumptions and limitations of our technique, as well as potential improvements:

Our inference assumes that the expression of the gene of interest is at steady state (Eq. (2)). While this assumption holds if the mRNA lifetimes are much shorter than the typical temporal changes that may affect the gene expression rates [1], there are situations where this would not be the case. For example, a liver metabolic gene that is highly responsive to feeding may have just been turned ON if the mouse has eaten within the last few minutes. In such situations we may observe many bright transcription sites but low numbers of cellular mRNA, since the cell has not yet had time to reach steady state. In such cases we may erroneously infer that the gene has highly unstable transcripts. Additional sources of variability may be circadian rhythms, physical activity and stress, which can yield temporally fluctuating transcription and degradation rates. To overcome this limitation it is recommended to sequentially sacrifice mice at several close time points (e.g. within an hour) and to examine the reproducibility of the inferred transcription and degradation rates on several mice at each time point.

Some genes are intron-less, e.g. many transcription factors, thus prohibiting the design of an intronic library. In these situations one can still use the exonic library to seek bright nuclear dots; however, this may lead to underestimation of the rates of genes with low transcription rate, where we might miss the dim TS dots. An alternative strategy to detect which nuclear exonic dots are active TS in such cases is to design probes against introns of highly transcribed genes that are located at close proximity on the same chromosome [38].

Our approach assumes that all nascent mRNA at the TS are physically attached to Pol2 molecules that are advancing at a constant rate. For genes that are long enough a single-molecule-based control experiment to validate this assumption is recommended [3].

Our estimates of TS intensities assume that they are diffraction-limited objects. In some situations (particularly for long genes) TS may actually encompass several voxels. In these cases it is recommended to quantify the total intensity of the TS rather than the integrated intensity at the brightest optical Z-section.

Eqs. (2) and (3) use the cytoplasmic levels of mRNA, since nuclear mRNA degradation is generally negligible. The pooled method uses all mRNA in the field of view instead of only the cytoplasmic mRNA, since the calculations are performed without cell segmentation. For most genes the levels of cytoplasmic mRNA will

be substantially higher than nuclear mRNA, however this is not always the case (Bahar Halpern et al., unpublished results). For genes with substantial nuclear retention the pooled approach may lead to under-estimation of the degradation rates. To overcome this, one can segment representative cells to estimate the fraction of total mRNA that is cytoplasmic and use this as a correction factor.

A fundamental limitation of the smFISH approach is that single molecule detection is currently unfeasible in thick tissues, due to the optical aberrations introduced by the tissue. A new set of technologies for tissue clearing [14,37,73,78] may alleviate this limitation, allowing single molecule detection in substantially thicker tissues.

Our Eqs. (1)–(5) neglect details of the stochastic processes of transcription and degradation, including promoter-coupled RNA degradation [18,25,74], promoter jamming [5,67,77] and refractory periods between bursts and degradation events [47,52,69,81]. Future elaborations on our method may facilitate inferring these additional important details.

8. Concluding remarks

The single-molecule FISH method described here is a generic technique to quantify the fundamental gene expression parameters of any gene of interest in defined sub-populations in an intact tissue. It enables assessment of differential regulation of gene expression through either modulation of transcription rates or mRNA stability and can facilitate description of how the tissue microenvironment affects these parameters. The ability to simultaneously measure distributions of single-cell mRNA counts further enables analysis of how transcription and degradation rates shape gene expression variability [3] and the single-cell statistics of TS can be used to tease out the relative contribution of extrinsic and intrinsic factors to this variability [3,59,70]. In addition, correlations between TS of different genes at the single-cell level can potentially uncover novel regulatory interactions and co-regulation [68]. Careful planning of smFISH libraries and analysis of their intensities can enable characterization not only of the average transcription rate but also the patterns of polymerase processivity and potential locations of polymerase pausing [3]. We believe this method can be a powerful technique that complements high-throughput methods for measuring transcription and degradation rates in mammalian tissues.

Acknowledgments

We thank Shanie Landen and all members of our lab for valuable comments on the manuscript. S.I. is the incumbent of the Philip Harris and Gerald Ronson Career Development Chair. We acknowledge support from the Henry Chanoch Krenter Institute for Biomedical Imaging and Genomics, The Leir Charitable Foundations, Richard Jakubskind Laboratory of Systems Biology, Cymerman-Jakubskind Prize, The Lord Sieff of Brimpton Memorial Fund, The Human Frontiers Science Program, the I-CORE program of the Planning and Budgeting Committee and the Israel Science Foundation, and the European Research Council under the European Union's Seventh Framework Programme (FP7/2007-2013)/ERC grant agreement number 335122.

Appendix A. Supplementary data

Supplementary data associated with this article can be found, in the online version, at http://dx.doi.org/10.1016/j.ymeth.2015.11.015.

References

[1] U. Alon, An Introduction to Systems Biology, Chapman & Hall/CRC, 2015.
[2] A. Ameur, A. Zaghlool, J. Halvardson, A. Wetterbom, U. Gyllensten, L. Cavelier, L. Feuk, Total RNA sequencing reveals nascent transcription and widespread co-transcriptional splicing in the human brain, Nat. Struct. Mol. Biol. 18 (2011) 1435–1440.
[3] K. Bahar Halpern, S. Tanami, S. Landen, M. Chapal, L. Szlak, A. Hutzler, A. Nizhberg, S. Itzkovitz, Bursty gene expression in the intact mammalian liver, Mol. Cell 58 (2015) 147–156.
[4] A. Bar-Even, J. Paulsson, N. Maheshri, M. Carmi, E. O'Shea, Y. Pilpel, N. Barkai, Noise in protein expression scales with natural protein abundance, Nat. Genet. 38 (2006) 636–643.
[5] C. Bécavin, M. Barbi, J.-M. Victor, A. Lesne, Transcription within condensed chromatin: steric hindrance facilitates elongation, Biophys. J. 98 (2010) 824–833.
[6] J.G. Belasco, G. Brawerman, 18 – Experimental approaches to the study of mRNA decay, in: J.G.B. Brawerman (Ed.), Control of Messenger RNA Stability, Academic Press, San Diego, 1993, pp. 475–493.
[7] E. Bertrand, P. Chartrand, M. Schaefer, S.M. Shenoy, R.H. Singer, R.M. Long, Localization of ASH1 mRNA particles in living yeast, Mol. Cell 2 (1998) 437–445.
[8] W.J. Blake, M. KÆrn, C.R. Cantor, J.J. Collins, Noise in eukaryotic gene expression, Nature 422 (2003) 633–637.
[9] W.J. Blake, G. Balázsi, M.A. Kohanski, F.J. Isaacs, K.F. Murphy, Y. Kuang, C.R. Cantor, D.R. Walt, J.J. Collins, Phenotypic consequences of promoter-mediated transcriptional noise, Mol. Cell 24 (2006) 853–865.
[10] K.S. Bloom, D.L. Beach, P. Maddox, S.L. Shaw, E. Yeh, E.D. Salmon, Using green fluorescent protein fusion proteins to quantitate microtubule and spindle dynamics in budding yeast, Methods Cell Biol. 61 (1999) 369–383.
[11] D.P. Bratu, B.-J. Cha, M.M. Mhlanga, F.R. Kramer, S. Tyagi, Visualizing the distribution and transport of mRNAs in living cells, Proc. Natl. Acad. Sci. USA 100 (2003) 13308–13313.
[12] L.A. Chodosh, A. Fire, M. Samuels, P.A. Sharp, 5,6-Dichloro-1-beta-D-ribofuranosylbenzimidazole inhibits transcription elongation by RNA polymerase II in vitro, J. Biol. Chem. 264 (1989) 2250–2257.
[13] S. Chong, C. Chen, H. Ge, X.S. Xie, Mechanism of transcriptional bursting in bacteria, Cell 158 (2014) 314–326.
[14] K. Chung, K. Deisseroth, CLARITY for mapping the nervous system, Nat. Methods 10 (2013) 508–513.
[15] L.S. Churchman, J.S. Weissman, Nascent transcript sequencing visualizes transcription at nucleotide resolution, Nature 469 (2011) 368–373.
[16] L.J. Core, J.J. Waterfall, J.T. Lis, Nascent RNA sequencing reveals widespread pausing and divergent initiation at human promoters, Science 322 (2008) 1845–1848.
[17] R.D. Dar, B.S. Razooky, A. Singh, T.V. Trimeloni, J.M. McCollum, C.D. Cox, M.L. Simpson, L.S. Weinberger, Transcriptional burst frequency and burst size are equally modulated across the human genome, Proc. Natl. Acad. Sci. USA 109 (2012) 17454–17459.
[18] M. Dori-Bachash, O. Shalem, Y.S. Manor, Y. Pilpel, I. Tirosh, Widespread promoter-mediated coordination of transcription and mRNA degradation, Genome Biol. 13 (2012) R114.
[19] A.M. Femino, F.S. Fay, K. Fogarty, R.H. Singer, Visualization of single RNA transcripts in situ, Science 280 (1998) 585–590.
[20] N. Friedman, L. Cai, X.S. Xie, Linking stochastic dynamics to population distribution: an analytical framework of gene expression, Phys. Rev. Lett. 97 (2006) 168302.
[21] G. Fuchs, Y. Voichek, S. Benjamin, S. Gilad, I. Amit, M. Oren, 4sUDRB-seq: measuring genomewide transcriptional elongation rates and initiation frequencies within cells, Genome Biol. 15 (2014) R69.
[22] N.L. Garneau, J. Wilusz, C.J. Wilusz, The highways and byways of mRNA decay, Nat. Rev. Mol. Cell Biol. 8 (2007) 113–126.
[23] C. Girard, C.L. Will, J. Peng, E.M. Makarov, B. Kastner, I. Lemm, H. Urlaub, K. Hartmuth, R. Lührmann, Post-transcriptional spliceosomes are retained in nuclear speckles until splicing completion, Nat. Commun. 3 (2012) 994.
[24] I. Golding, J. Paulsson, S.M. Zawilski, E.C. Cox, Real-time kinetics of gene activity in individual bacteria, Cell 123 (2005) 1025–1036.
[25] G. Haimovich, M. Choder, R.H. Singer, T. Trcek, The fate of the messenger is pre-determined: a new model for regulation of gene expression, Biochim. Biophys. Acta BBA – Gene Regul. Mech. 1829 (2013) 643–653.
[26] S. Harrold, C. Genovese, B. Kobrin, S.L. Morrison, C. Milcarek, A comparison of apparent mRNA half-life using kinetic labeling techniques vs decay following administration of transcriptional inhibitors, Anal. Biochem. 198 (1991) 19–29.
[27] S. Itzkovitz, A. van Oudenaarden, Validating transcripts with probes and imaging technology, Nat. Methods 8 (2011) S12–S19.
[28] S. Itzkovitz, A. Lyubimova, I.C. Blat, M. Maynard, J. van Es, J. Lees, T. Jacks, H. Clevers, A. van Oudenaarden, Single-molecule transcript counting of stem-cell markers in the mouse intestine, Nat. Cell Biol. 14 (2012) 106–114.
[29] S. Itzkovitz, I.C. Blat, T. Jacks, H. Clevers, A. van Oudenaarden, Optimality in the development of intestinal crypts, Cell 148 (2012) 608–619.
[30] C.Y. Jao, A. Salic, Exploring RNA transcription and turnover in vivo by using click chemistry, Proc. Natl. Acad. Sci. USA 105 (2008) 15779–15784.
[31] I. Jonkers, J.T. Lis, Getting up to speed with transcription elongation by RNA polymerase II, Nat. Rev. Mol. Cell Biol. 16 (2015) 167–177.

[32] J.P. Junker, A. van Oudenaarden, Every cell is special: genome-wide studies add a new dimension to single-cell biology, Cell 157 (2014) 8–11.
[33] M. Kærn, T.C. Elston, W.J. Blake, J.J. Collins, Stochasticity in gene expression: from theories to phenotypes, Nat. Rev. Genet. 6 (2005) 451–464.
[34] A.M. Khalil, M. Guttman, M. Huarte, M. Garber, A. Raj, D. Rivea Morales, K. Thomas, A. Presser, B.E. Bernstein, A. van Oudenaarden, et al., Many human large intergenic noncoding RNAs associate with chromatin-modifying complexes and affect gene expression, Proc. Natl. Acad. Sci. USA 106 (2009) 11667–11672.
[35] Y.L. Khodor, J. Rodriguez, K.C. Abruzzi, C.-H.A. Tang, M.T. Marr, M. Rosbash, Nascent-seq indicates widespread cotranscriptional pre-mRNA splicing in Drosophila, Genes Dev. 25 (2011) 2502–2512.
[36] Y.L. Khodor, J.S. Menet, M. Tolan, M. Rosbash, Cotranscriptional splicing efficiency differs dramatically between Drosophila and mouse, RNA (NY) 18 (2012) 2174–2186.
[37] S.-Y. Kim, K. Chung, K. Deisseroth, Light microscopy mapping of connections in the intact brain, Trends Cognit. Sci. 17 (2013) 596–599.
[38] M.J. Levesque, A. Raj, Single-chromosome transcriptional profiling reveals chromosomal gene expression regulation, Nat. Methods 10 (2013) 246–248.
[39] S.C. Little, M. Tikhonov, T. Gregor, Precise developmental gene expression arises from globally stochastic transcriptional activity, Cell 154 (2013) 789–800.
[40] E. Lubeck, L. Cai, Single-cell systems biology by super-resolution imaging and combinatorial labeling, Nat. Methods 9 (2012) 743–748.
[41] A. Lyubimova, S. Itzkovitz, J.P. Junker, Z.P. Fan, X. Wu, A. van Oudenaarden, Single-molecule mRNA detection and counting in mammalian tissue, Nat. Protoc. 8 (2013) 1743–1758.
[42] H. Maamar, A. Raj, D. Dubnau, Noise in gene expression determines cell fate in *Bacillus subtilis*, Science 317 (2007) 526–529.
[43] A. Mayer, J. di Iulio, S. Maleri, U. Eser, J. Vierstra, A. Reynolds, R. Sandstrom, J.A. Stamatoyannopoulos, L.S. Churchman, Native elongating transcript sequencing reveals human transcriptional activity at nucleotide resolution, Cell 161 (2015) 541–554.
[44] C. Mayr, D.P. Bartel, Widespread shortening of 3′UTRs by alternative cleavage and polyadenylation activates oncogenes in cancer cells, Cell 138 (2009) 673.
[45] J.S. Menet, J. Rodriguez, K.C. Abruzzi, M. Rosbash, Nascent-Seq reveals novel features of mouse circadian transcriptional regulation, eLife 1 (2012).
[46] E.C. Merkhofer, P. Hu, T.L. Johnson, Introduction to cotranscriptional RNA splicing, Methods Mol. Biol. (Clifton, NJ) 1126 (2014) 83–96.
[47] N. Molina, D.M. Suter, R. Cannavo, B. Zoller, I. Gotic, F. Naef, Stimulus-induced modulation of transcriptional bursting in a single mammalian gene, Proc. Natl. Acad. Sci. USA 110 (2013) 20563–20568.
[48] R. Monroy-Contreras, L. Vaca, Molecular beacons: powerful tools for imaging RNA in living cells, J. Nucleic Acids 2011 (2011) e741723.
[49] J.R.S. Newman, S. Ghaemmaghami, J. Ihmels, D.K. Breslow, M. Noble, J.L. DeRisi, J.S. Weissman, Single-cell proteomic analysis of *S. cerevisiae* reveals the architecture of biological noise, Nature 441 (2006) 840–846.
[50] T. Nojima, T. Gomes, A.R.F. Grosso, H. Kimura, M.J. Dye, S. Dhir, M. Carmo-Fonseca, N.J. Proudfoot, Mammalian NET-seq reveals genome-wide nascent transcription coupled to RNA processing, Cell 161 (2015) 526–540.
[51] O. Padovan-Merhar, G.P. Nair, A.G. Biaesch, A. Mayer, S. Scarfone, S.W. Foley, A. R. Wu, L.S. Churchman, A. Singh, A. Raj, Single mammalian cells compensate for differences in cellular volume and DNA copy number through independent global transcriptional mechanisms, Mol. Cell 58 (2015) 339–352.
[52] J.M. Pedraza, J. Paulsson, Effects of molecular memory and bursting on fluctuations in gene expression, Science 319 (2008) 339–343.
[53] E. Querido, P. Chartrand, Using fluorescent proteins to study mRNA trafficking in living cells, Methods Cell Biol. 85 (2008) 273–292.
[54] M. Rabani, J.Z. Levin, L. Fan, X. Adiconis, R. Raychowdhury, M. Garber, A. Gnirke, C. Nusbaum, N. Hacohen, N. Friedman, et al., Metabolic labeling of RNA uncovers principles of RNA production and degradation dynamics in mammalian cells, Nat. Biotechnol. 29 (2011) 436–442.
[55] B. Rädle, A.J. Rutkowski, Z. Ruzsics, C.C. Friedel, U.H. Koszinowski, L. Dölken, Metabolic labeling of newly transcribed RNA for high resolution gene expression profiling of RNA synthesis, processing and decay in cell culture, J. Vis. Exp. (JoVE) (2013).
[56] A. Raj, A. van Oudenaarden, Nature, nurture, or chance: stochastic gene expression and its consequences, Cell 135 (2008) 216–226.
[57] A. Raj, C.S. Peskin, D. Tranchina, D.Y. Vargas, S. Tyagi, Stochastic mRNA synthesis in mammalian cells, PLoS Biol. 4 (2006) e309.
[58] A. Raj, P. van den Bogaard, S.A. Rifkin, A. van Oudenaarden, S. Tyagi, Imaging individual mRNA molecules using multiple singly labeled probes, Nat. Methods 5 (2008) 877–879.
[59] J.M. Raser, E.K. O'Shea, Noise in gene expression: origins, consequences, and control, Science 309 (2005) 2010–2013.
[60] J. Rodriguez, J.S. Menet, M. Rosbash, Nascent-seq indicates widespread cotranscriptional RNA editing in Drosophila, Mol. Cell 47 (2012) 27–37.
[61] J. Ross, mRNA stability in mammalian cells, Microbiol. Rev. 59 (1995) 423–450.
[62] J. Schindelin, I. Arganda-Carreras, E. Frise, V. Kaynig, M. Longair, T. Pietzsch, S. Preibisch, C. Rueden, S. Saalfeld, B. Schmid, et al., Fiji: an open-source platform for biological-image analysis, Nat. Methods 9 (2012) 676–682.
[63] B. Schwanhäusser, D. Busse, N. Li, G. Dittmar, J. Schuchhardt, J. Wolf, W. Chen, M. Selbach, Global quantification of mammalian gene expression control, Nature 473 (2011) 337–342.
[64] O. Shalem, O. Dahan, M. Levo, M.R. Martinez, I. Furman, E. Segal, Y. Pilpel, Transient transcriptional responses to stress are generated by opposing effects of mRNA production and degradation, Mol. Syst. Biol. 4 (2008) 4.
[65] S.O. Skinner, L.A. Sepúlveda, H. Xu, I. Golding, Measuring mRNA copy number in individual *Escherichia coli* cells using single-molecule fluorescent in situ hybridization, Nat. Protoc. 8 (2013) 1100–1113.
[66] L.-H. So, A. Ghosh, C. Zong, L.A. Sepúlveda, R. Segev, I. Golding, General properties of transcriptional time series in *Escherichia coli*, Nat. Genet. 43 (2011) 554–560.
[67] R. Sousa, Tie me up, tie me down: inhibiting RNA polymerase, Cell 135 (2008) 205–207.
[68] J. Stewart-Ornstein, J.S. Weissman, H. El-Samad, Cellular noise regulons underlie fluctuations in *Saccharomyces cerevisiae*, Mol. Cell 45 (2012) 483–493.
[69] D.M. Suter, N. Molina, D. Gatfield, K. Schneider, U. Schibler, F. Naef, Mammalian genes are transcribed with widely different bursting kinetics, Science 332 (2011) 472–474.
[70] P.S. Swain, M.B. Elowitz, E.D. Siggia, Intrinsic and extrinsic contributions to stochasticity in gene expression, Proc. Natl. Acad. Sci. USA 99 (2002) 12795–12800.
[71] R.Z. Tan, A. van Oudenaarden, Transcript counting in single cells reveals dynamics of rDNA transcription, Mol. Syst. Biol. 6 (2010) 358.
[72] H. Tilgner, D.G. Knowles, R. Johnson, C.A. Davis, S. Chakrabortty, S. Djebali, J. Curado, M. Snyder, T.R. Gingeras, R. Guigó, Deep sequencing of subcellular RNA fractions shows splicing to be predominantly co-transcriptional in the human genome but inefficient for lncRNAs, Genome Res. 22 (2012) 1616–1625.
[73] R. Tomer, L. Ye, B. Hsueh, K. Deisseroth, Advanced CLARITY for rapid and high-resolution imaging of intact tissues, Nat. Protoc. 9 (2014) 1682–1697.
[74] T. Trcek, D.R. Larson, A. Moldón, C.C. Query, R.H. Singer, Single-molecule mRNA decay measurements reveal promoter regulated mRNA stability in yeast, Cell 147 (2011) 1484–1497.
[75] S. Tyagi, F.R. Kramer, Molecular beacons: probes that fluoresce upon hybridization, Nat. Biotechnol. 14 (1996) 303–308.
[76] S. Tyagi, D.P. Bratu, F.R. Kramer, Multicolor molecular beacons for allele discrimination, Nat. Biotechnol. 16 (1998) 49–53.
[77] Z. Waks, P.A. Silver, Nuclear origins of cell-to-cell variability, Cold Spring Harb. Symp. Quant. Biol. 75 (2010) 87–94.
[78] B. Yang, J.B. Treweek, R.P. Kulkarni, B.E. Deverman, C.-K. Chen, E. Lubeck, S. Shah, L. Cai, V. Gradinaru, Single-cell phenotyping within transparent intact tissue through whole-body clearing, Cell 158 (2014) 945–958.
[79] A. Zeisel, W.J. Köstler, N. Molotski, J.M. Tsai, R. Krauthgamer, J. Jacob-Hirsch, G. Rechavi, Y. Soen, S. Jung, Y. Yarden, et al., Coupled pre-mRNA and mRNA dynamics unveil operational strategies underlying transcriptional responses to stimuli, Mol. Syst. Biol. 7 (2011).
[80] D. Zenklusen, D.R. Larson, R.H. Singer, Single-RNA counting reveals alternative modes of gene expression in yeast, Nat. Struct. Mol. Biol. 15 (2008) 1263–1271.
[81] B. Zoller, D. Nicolas, N. Molina, F. Naef, Structure of silent transcription intervals and noise characteristics of mammalian genes, Mol. Syst. Biol. 11 (2015).